CALIFORNIA STATE UNIVERSITY, NORTHRIDGE

Minimization of Torque Ripple in Permanent Magnet Synchronous Motors Through Direct Torque Control

A graduate project submitted in partial fulfillment of the requirements

For the degree of Master of Science in Electrical Engineering

By

Kevin N.L. Heward-Mills

August 2018

The Graduate Project of Kevin N.L. Heward-Mills is approved:

_____	_____
Xiyi Hang, PhD	Date
_____	_____
John Valdovinos, PhD	Date
_____	_____
Professor Ignacio B. Osorno, Chair	Date

California State University, Northridge

Table of Contents

List of Figures

Abstract

Minimization of Torque Ripple in Permanent Magnet Synchronous Motors through Direct Torque Control

By

Kevin N.L. Heward-Mills

Master of Science in Electrical Engineering

Permanent Magnet motors are of pertinent use in factory automation, machine tool applications, electric vehicles, robotics applications and many others. Within these industries, the measure of accuracy that is required on a constant basis is stymied by the common obstacle of harmonic ripple in torque, caused by discrepancies in flux within the air-gap of the motors. This ripple reflects in performance of the motor drive and consequently causes a harmonic disturbance in stator current. In order to understand this phenomenon and come about various remedial practices, a detailed study is carried out in this project to investigate the causes of torque ripple in permanent magnet synchronous motor drives, and the methods used in the minimization of this ripple. Minimization of these ripples in torque would prove essential to save erroneous manufacturing deviations that they characterize in the above-mentioned industry applications. It would also help in saving industrial financial resources, increase reliability, as well as save time spent in corrections of these errors. A model is presented in MATLAB/Simulink to implement the Direct Torque approach of ripple minimization.

CHAPTER 1

Introduction

The widespread application of permanent magnet motor drives highlights their importance. Whether in industrial servo applications, spindle drives for machine tools, positioning systems, robotics, electric vehicle applications among many others, it is important to maintain optimum efficiency and a consistent precision in operation so as to prevent unwanted, and potentially disastrous repercussions.

Permanent magnet synchronous motor drives, hereafter referred to as PMSM drives, are at times preferred over dc-excited motors. This is due to the fact that the application of PMSM drives results in less copper losses, since there are no individual excitation windings involved with rotor operation. This lack of excitation windings also contributes to a reduction in losses, that otherwise would have been produced by winding magnetizing currents. In turn, PMSM motors are more efficient, and more powerful by virtue of their high flux densities due to the use of powerful rare-earth magnets [4].

Permanent magnet motors are also preferred over dc-excited motors since the presence of magnets in the rotors eliminate the need for continuous supply of electrical energy to sustain flux operation. Since there is a lack of windings in the layout of the IPM rotor, there is not only a maintenance of magnetic flux due to the presence of permanent magnets, but there is also an improvement in the weight of the motor drive since the bulkiness of rotor windings is eliminated from ergonomic consideration. This thereby results in a more desirable power density. Another factor that is also considered is the improved operation of permanent magnet motors in higher temperatures, since there are less windings and copper losses.

In contrast to these advantages, a disadvantage in the application of PMSM drives is the expense involved. The rare-earth magnets such as Neodymium and Samarium Cobalt [8] are permanently fixed onto the rotor. These are limited, perishable resources, and are therefore expensive in acquisition. The complexities involved in the circuit topology, also limit the number of applications possible by the implementation of these motor drives.

An issue that remains in the application of PMSM motor drives is the presence of oscillations of torque that reflect throughout the system in the form of ripples in stator current and machine torque. This is as a result of the saliency in the rotor structure, which causes slight discrepancies in the flux density within the air gap, as the rotor position changes continually. There is also a variance in magnetic reluctance within the air gap and this is caused by layout of the stator slots. Since there is a non-uniformity of torque distribution in such a case, the ripple in torque during operation results in deviations in speed and efficiency during applications. Apart from these oscillations in speed, there may also be a production of noise due to a trigger of resonance in mechanical components of the motor drive.

Interior permanent magnet motors are usually categorized by the waveform of their back electromotive force (EMF) and these are usually two categories; namely trapezoidal and sinusoidal back EMF waveform motor drives. Trapezoidal motors have their name by virtue of the trapezoidal waveform of back EMF. To obtain a constant torque regardless of the position of the revolving rotor, the stator would require rectangular current waveforms. In sinusoidal IPM motors, the torque in the air gap owes mostly to the quadrature component of armature current. There is also the existence of reluctance torque, which is proportional to the products of direct and quadrature axis currents. The harmonic components of torque arise from non-sinusoidal flux linkages to the stator, and other harmonic ripples in the stator current waveform. It is important to note however, that ripple in torque is still considerably less frequent in sinusoidal motor drives than with trapezoidal back EMF motor drives, and are therefore more popularly utilized [4].

Torque pulsations may be mitigated or eliminated by the implementation of specific stator-winding layouts, or the modulation of excitation currents in the stator. In the case of the latter, the lower frequency torque ripples are negated by an inverse component of torque that is obtained through the modulation of stator current. This modulated stator current is specified based on analysis of the waveform of the machine back EMF.

Literature Review

Liu et al investigated the process of "active" control in [1]. Regarding this process, voltage or current fed into the stator of the PMSM drive is altered by virtue of a specifically designed controller. This controller is aimed at the vitiation of torque deviations that may occur. The use of this controller is meant to be integrated into the servomotor system of the PMSM drive, and is therefore specified to work across different types of motor drives. A look-up table is introduced to enable switching of current/voltage values that are being 'modulated' into the stator. Such an approach would however require exact parameters of the involved motor, corresponding to the motor type. This includes the affinity that corresponds between pulsations in torque and the excitation currents required of the stator. Failure to acquire these predetermined factors would result in error signal deviations, which could worsen the ripples in torque. Iterative learning control was the approach used in [1], where a speed controller typically works with a proportional-integral (PI) controller, to offset the deviation about the reference current and consequently attenuate the ripple in torque. The issue that arose with this case was with respect to the resilience of the system, which rested on the acuteness of the system in response to changes in parameters or outside factors such as load perturbations. Iterative learning control is a good choice in periodically rippled systems [1].

In [2], the method of direct torque control is of primary focus, executed conventionally. A conclusion is arrived at, establishing that direct torque execution would result in a relatively uncomplicated designated controller, which develops a resiliency against slight variations in motor parameters. This method however engenders a variable switching frequency and remaining ripples in torque seem to be high. These factors are as a result of the implementation of hysteresis-based comparators, which use error signals between

measured and reference torque/flux to govern the logic of switching. To remedy this issue, it is possible to generate an algorithm that that individually computes hysteresis bands for torque and flux, thereby mitigating the high ripples that may be obtained. It still stands that the system remains sensitive to slight variations in motor characteristics and thus reduces efficiency immensely [2].

A method of maintaining switching frequency as constantly as possible is proposed in [19], where the direct torque method of control is modified to replace the hysteresis band comparators or switching table method with space vector modulation. This brings about the advantage of low ripples in torque s well as a nearly constant switching frequency. Furthermore, the direct-axis current into the stator when the machine is operated at varied load is reduced to maintain a uniform stator flux. The disadvantage of this approach remains that a relatively high computing power is required for the algorithm to take effect [19].

Objectives

This paper aims at the following objectives in the sections following:

- The juxtaposition between Field Oriented Control and Direct Torque Control in torque-ripple minimization within permanent magnet synchronous motors.
- The analysis and implementation of Space Vector Pulse Width Modulation
- Design and simulation of Direct Torque implementation in the minimization of torque ripple.
- Analysis of the performance of said simulation.

CHAPTER 2

Permanent Magnet Motor Topology & Layout

Regarding permanent magnet synchronous motors with sinusoidal back-EMF, stator windings are required to be laid out about the air-gap such that a sinusoidal waveform of electromotive force. Consequently, the flux density generated about the air-gap by the magnets alternates in a sinusoidal fashion. The dynamics of the rotor involved in this machine are either based on the surface-mounted or interior magnet topology [7].

Figure 1 provides a structural juxtaposition between surface-mounted permanent magnet and interior permanent magnet configurations. As illustrated, the black portions represent the magnet positions that produce a sinusoidal flux.

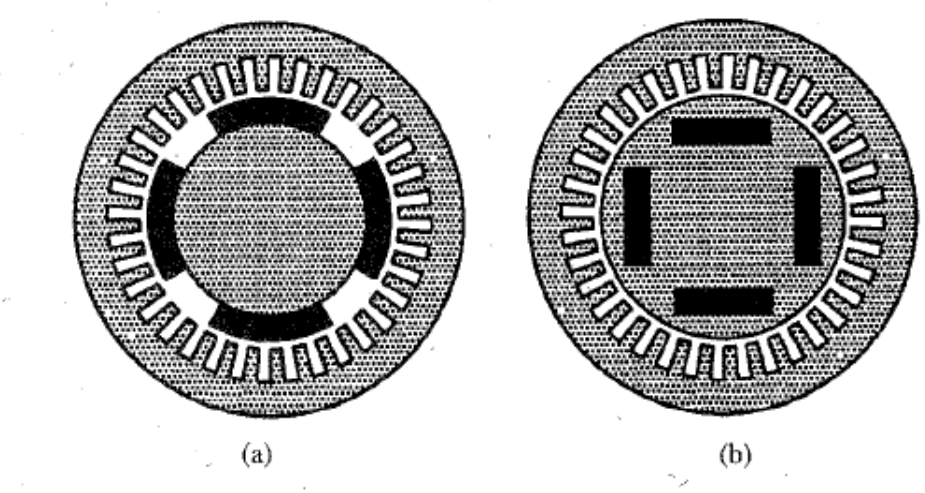

Figure 1: Cross-Sectional Views of (a) Surface-Mounted Permanent Magnet Motors (b) Interior Permanent Magnet Motors [7]

Torque Ripple

With so many varying applications of permanent magnet AC motor drives, the consistency in torque provided by these machines makes all the difference in providing smooth, efficient and desirable results. The mitigation of pulsating effects of undesirable harmonic components of torque therefore is of importance to efficiency of the motor drive system.

As per the sources of fluctuating torque, T.M. Jahns et al (1996) explained, "Any source of divergence from ideal conditions in either motor or associated power converter in a Permanent Magnet AC motor drive gives rise to undesired torque pulsations". It was further explained that these discrepancies in torque could be categorized into three

groups. Within the first category, it was explained that the disparity between the magnetic flux in the rotor and the deviations in magnetic reluctance in the stator, interplay to give rise to Cogging Torque. Another category known as Ripple Torque, had to do with the action of magneto-motive force of stator current with electromagnetic characteristics produced by rotor action. These characteristics took the form of "mutual" torque that spurred from the magneto-motive forces of stator current, acting on flux of the rotor, and "reluctance" torque, which was a product of the same magneto-motive force with the deviation in angle of the rotor magnetic reluctance. The resultant of these two forces gave rise to the defined pulsating torque [7].

In order to mitigate the fluctuations given by these torque components, there exist two dichotomies of approaches used. One such approach exists, involving improvement in ergonomics within the architecture of the Permanent Magnet AC motor drive such that its attributes are more optimal in nature. Even though such an approach would be considered the most efficient method of mitigating torque ripple, it faces the challenge of high costs involved with construction. In addition, this would not serve an effective approach for many existing designed machines. Nevertheless, in construction of Permanent Magnet AC motor drives, design considerations such as the alteration of lamination stacks within the stator, and the use of fractional slot-pitch windings prove useful [7].

Another approach, which is of interest in this paper, is the use of control schemes that compensate for discrepancies in excitation current in the stator. In the implementation of this approach, motor drive schematics and parameters are required. This approach is more practical for machines with low cost involved in manufacture, and is commonly preferred.

CHAPTER 3

Mathematical Model And Characteristics Of PMSM

It is a common convention for the state equations of permanent magnet synchronous motors to be expressed in the rotor synchronous reference frame. This is because sinusoidal quantities reflect as constant parameters in steady state conditions. Thus the equations of a PMSM with an induced sinusoidal back EMF, assuming negligible hysteresis and eddy current losses are represented as [6]:

$$v_d = R_s i_d + \frac{d}{dt}\psi_d - \omega_r \psi_q \tag{1}$$

$$v_q = R_s i_q + \frac{d}{dt}\psi_q - \omega_r \psi_d \tag{2}$$

$$\psi_d = L_d i_d + \psi_f \tag{3}$$

$$\psi_q = L_q i_q \tag{4}$$

Where v_d and v_q are the respective direct and quadrature axes stator voltages, R_s is the stator resistance, ψ_d and ψ_q are the direct and quadrature axes stator fluxes respectively, ω_r is the rotor speed, i_d and i_q are the direct and quadrature axes stator currents respectively, L_d and L_q respectively represent the direct and quadrature axes stator inductance, and ψ_f represents the flux linkage created by the permanent magnet. The electromagnetic torque developed within the air gap is represented by:

$$T_e = \frac{3}{2} p(\psi_d i_q - \psi_q i_d) \tag{5}$$

Where p is the number of pole pairs. From these relations, the machine torque may be adjusted by the varying of stator current in the d and q axes frame of reference. The dynamics of the PMSM are represented by the equation:

$$J\frac{d\omega_m}{dt} = T_e - T_L - B\omega_m \tag{6}$$

Thus, the mechanical speed of the rotor can be surmised from equation 6 by solving for ω_m using the relation:

$$\omega_m = \int (\frac{T_e - T_L - B\omega_m}{J})dt \quad (7)$$

Where J represents inertia, ω_m is the mechanical angular velocity, B is known as the frictional coefficient and T_L is the load torque. Thus, by this dynamic and equations previously given, the output torque is maximized by the field-oriented control approach when the d-axis current is kept at zero [1].

Based on the d-q frame of rotation, an equivalent circuit illustrates the characteristic effects of the permanent magnet synchronous machine as the rotor revolves. In Figure 2 below, the circuits illustrated are based on equations (1) to (4), where P represents the number of poles, with the vector symbol Φ replacing ψ as magnetic flux within the air gap [12].

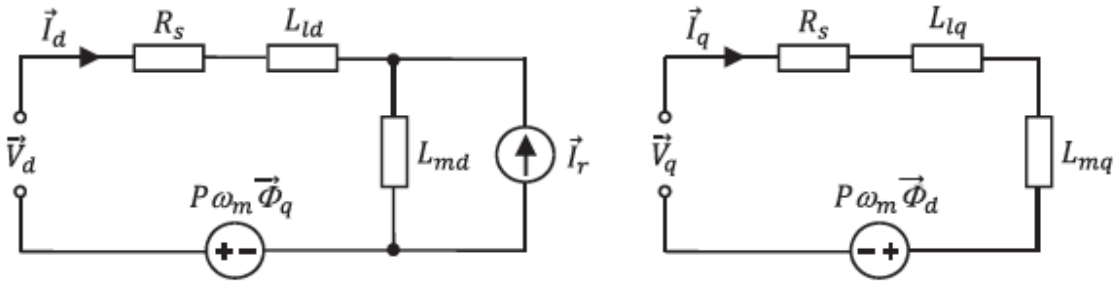

Figure 2: Equivalent d-q Circuit of PMSM in the Rotating Frame [12]

The symbols L_{ld} and L_{md} represent the leakage and magnetizing inductances, where they both contribute to the total inductance in the d-q frame. This is shown as [12]:

$$\boldsymbol{L_d = L_{ld} + L_{md}} \quad \textbf{(8)}$$

$$\boldsymbol{L_q = L_{lq} + L_{mq}} \quad \textbf{(9)}$$

$$\boldsymbol{\psi_f = L_{md} \cdot i_r} \quad \textbf{(10)}$$

The vector i_r signifies a current source, which supplies the rotor magnets, and is constant.

CHAPTER 4

The Park & Clarke Transformations

In electrical machine engineering, there is often the need to generate two-axis frames of reference due to the rotating nature of machine operations. This is to reconcile sinusoidal three-phase power into either a rotating or stationary reference.

The Clarke transformation, which was originated by Edith Clarke, serves as a useful method of transforming three-phase circuits and variables into a stationary reference frame. The orthogonal axes of this frame are expressed as α as the abscissa and β on the ordinate.

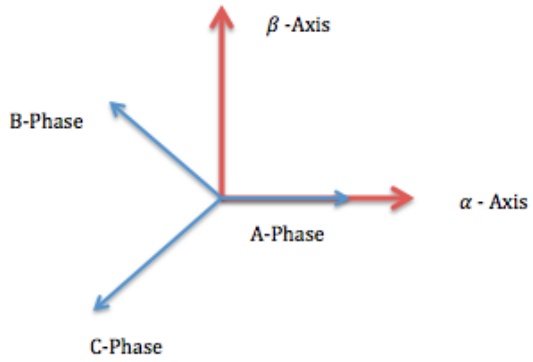

Figure 3: Three-Phase into Orthogonal Two-Phase Axes by Clarke Transformation

In figure 3 above, the transformation uses phase a as a reference and thus [17]:

$$v_\alpha = v_a \tag{11}$$

$$v_\beta = \frac{2v_b + v_a}{\sqrt{3}}$$

To be able to convert back to the three-phase frame, the zero sequence is incorporated into the operation, where *x* represents the variables under transformation, namely voltage, current, flux linkages or electric charge [17]:

$$[x_{\alpha\beta 0}] = T_{\alpha\beta 0}[x_{abc}]$$

$$T_{\alpha\beta 0} = \frac{2}{3}\begin{bmatrix} 1 & -1/2 & -1/2 \\ 0 & \sqrt{3}/2 & -\sqrt{3}/2 \\ 1/2 & 1/2 & 1/2 \end{bmatrix} \tag{12}$$

Therefore, inverse Clarke transformation is expressed by:

$$[x_{\alpha\beta 0}] = T_{\alpha\beta 0}^{-1}[x_{abc}] \tag{13}$$

$$T_{\alpha\beta 0}^{-1} = \begin{bmatrix} 1 & 0 & 1 \\ -1/2 & \sqrt{3}/2 & 1 \\ -1/2 & -\sqrt{3}/2 & 1 \end{bmatrix}$$

A graphical representation of current transformation and it's equations will follow shortly when it's use is highlighted in field oriented control.

The Park transformation was first brought to light in the early 1920s by Robert H. Park, and was practiced in analyzing electrical machinery. Park associated changes in variables with virtual windings in rotation with the rotor. This allowed him to base these variables on a d-q rotating reference frame that moved as if it was fixed to the rotor. This approach allowed the elimination of time-varying inductances in sinusoidal voltages of three-phase machines with the rotor in operation, since all variables are considered constant from the rotor as reference point of view [17].

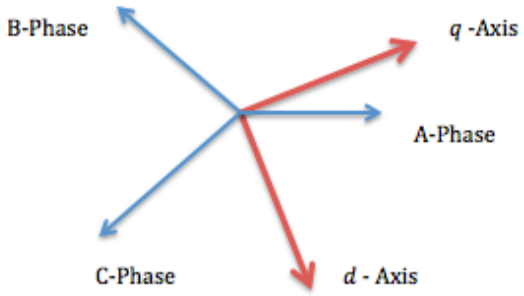

Figure 4: Transformation of 3-Phase to Two-Phase Rotating Frame

The equations governing the Park transformation are illustrated below [17]:

$$[y_{qd0}] = T_{qd0}(\theta)[y_{abc}] \tag{14}$$

$$T_{qd0}(\theta) = \frac{2}{3}\begin{bmatrix} \cos\theta & \cos(\theta - 2\pi/3) & \cos(\theta + 2\pi/3) \\ \sin\theta & \sin(\theta - 2\pi/3) & \sin(\theta + 2\pi/3) \\ 1/2 & 1/2 & 1/2 \end{bmatrix}$$

Where θ represents the rotor position in the park frame of reference. An inverse of this is also important, where it is shown that [17]:

$$[y_{abc}] = T_{qd}^{-1}(\theta)[y_{qd0}] \tag{15}$$

$$T_{qd}^{-1}(\theta) = \begin{bmatrix} \cos\theta & \sin\theta & 1 \\ \cos(\theta - {}^{2\pi}/_{3}) & \sin(\theta - {}^{2\pi}/_{3}) & 1 \\ \cos(\theta + {}^{2\pi}/_{3}) & \sin(\theta + {}^{2\pi}/_{3}) & 1 \end{bmatrix}$$

CHAPTER 5

Methods Of Control

The approaches involved with control of torque within PMSM drives are usually based on variable frequency control with the use of vectors. There are varying elements involved with each type, but the focus in this paper is going to be primarily on two popular methodologies, namely:

- Field Oriented Control
- Direct Torque Control

An emphasis in this paper is placed on the latter. Direct Torque control conventionally is split into various types as is shown in the following figure below, however the most popular method involving space vector modulation (DTC SVM) is of interest in this case.

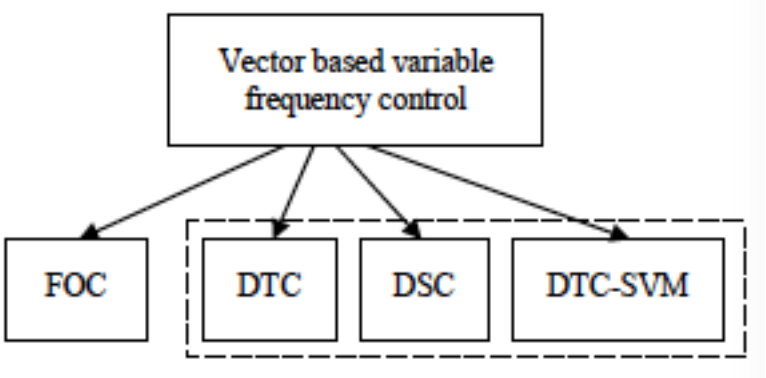

Figure 5: Classifications of Popular Vector-Based PMSM Control Methods [8]

Field Oriented Control

This is a popular method of vector control that involves the representation of a vector that is used in the modulation of stator current. It involves the transformation of a three-phase system into the direct and quadrature components, whereby torque is associated with the q-coordinate and flux is associated with the d-coordinate. This contributes to the facilitation of implementation of torque adjustment [5].

Since the stator current is decoupled into torque and flux components in the rotational reference frame, the following advantages follow for this method of control:

- The complexity of three phase currents is resolved into a more simple and linear system.
- Increased efficiency
- It allows for individual modulation of torque and flux, as with dc motors.

In order to decouple the three-phase stator currents into components that allow for the variation of torque, a transformation is required, first into the orthogonal two-phase stationary ($\alpha - \beta$) reference frame, then into the d-q rotating reference frame.

For the sustainment of an optimum torque that is commensurate to a certain stator current, this said current must be aligned with the quadrature axis such that the direct axis stator current is at zero [8].

Thus, the transformations are shown below, where:

$$i_{s\alpha} = i_a \tag{16}$$

$$i_{s\beta} = \frac{1}{\sqrt{3}} i_a + \frac{2}{\sqrt{3}} i_b \tag{17}$$

Equations (16) and (17) are based on the assumption that the phase-a axis and the α-axis are in the same phase. Thus a space vector diagram representation would follow as in figure 1 below.

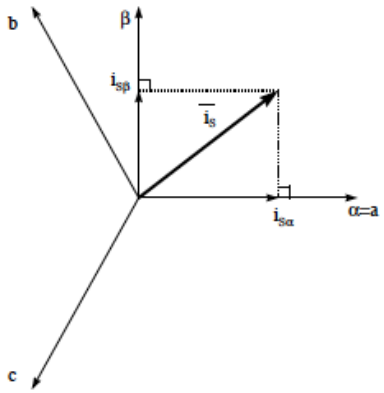

Figure 6: Stator Current Space Vector & Components (a-b and $\alpha - \beta$) [5]

The above diagram depicts the space vector relation between stator current and the three phase sinusoidal system. The transformation of three-phase current into the orthogonal frame of reference is known as the Clarke Transformation.

This transformation is further adjusted from a two-dimension orthogonal frame to a two-dimension rotating frame of reference by the Park Transformation, which is deduced by equations 10 and 11 shown below:

$$i_{sd} = i_{s\alpha} \cos\theta + i_{s\beta} \sin\theta \tag{18}$$

$$i_{sq} = i_{s\alpha} \sin\theta + i_{s\beta} \cos\theta \tag{19}$$

The angle, θ, represents the angular position of rotor and its corresponding direction of flux in the air gap. This angle is usually obtained via a position sensor. From these relations, it is possible to make a transformation into rotating d-q components, with which modification of torque is facilitated. With the assumption that the direct axis is in phase with rotor flux the resulting phase diagram depiction between both two-dimensional frames of reference follows simultaneously in the figure below [5].

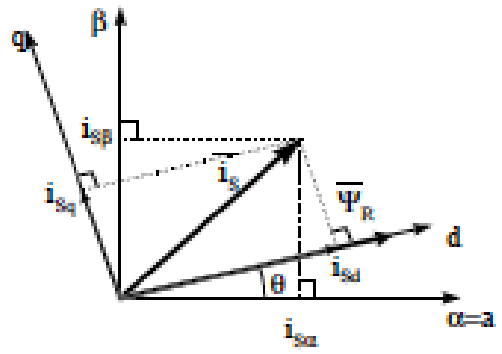

Figure 7: Space Vector Phasor Representation of Stator Current in Orthogonal and d-q Rotating Reference [5]

For the completion of the modification of torque via these two-dimension coordinate systems, a voltage vector transformation is required to create a reference voltage vector, which is pertinent to the space vector pulse-width modulation. The inverse Park Transform is thus applied to the controlled direct and quadrature voltages, which are modified using the transformed respective stator currents previously obtained. The reference voltages in the direct and quadrature axes respectively, are therefore deduced by:

$$V_{\alpha ref} = V_{dref} \cos\theta - V_{qref} \sin\theta \tag{20}$$

$$V_{\beta ref} = V_{dref} \sin\theta + V_{qref} \cos\theta \tag{21}$$

A block diagram model of Field oriented Control of PMSM drives is shown in Figure 8 [8]:

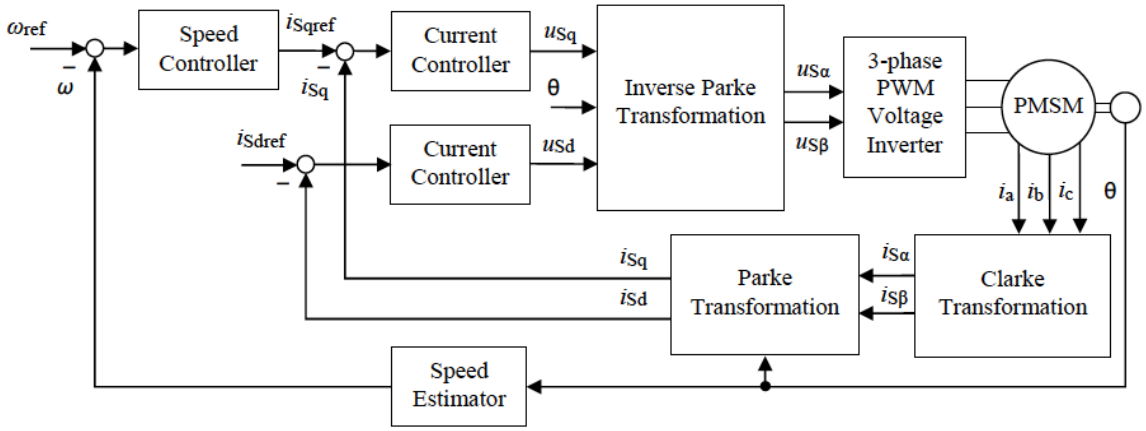

Figure 8: Field Oriented Control Block Diagram Model [8]

Despite the good measure of efficiency, the main disadvantage of the Field Oriented approach of torque control owes to the volatility of the system in certain situations. This may be as a result of potential modifications in motor parameters, as well as perturbations that may arise amid motor action. Another contribution to such instability may be as a result of computed bounds in speed control, whereby a breach leads to instability [8].

Direct Torque Control

The fundamental dynamic of Direct Torque control involves the process of choosing an optimum vector that represents the best choice of stator voltage that is appropriate for manipulation of torque within the machine. This is usually as a result of error measurement between reference values of stator torque and flux linkage, and their measured values [9].

This involves the implementation of Space Vector Pulse Width Modulation, whereby the most suitable space vectors of stator voltage are adopted in accordance with the state of error between approximate values of torque and flux, and their respective references. The approximation of stator torque and flux depend on the measured values obtained from the terminals of the motor. Within the six available voltage space vectors, the most ideal vector is chosen.

Direct Torque control is considered the best alternative for use in brushless dc motors, and as such is popular in that regard. There exists a modification to the conventional direct torque however, since it is established that the conventional direct torque scheme involving switching tables by virtue of the hysteresis controller, results in a larger measure of harmonic ripple in torque and flux. As a control measure, the implementation of a Proportional Integral (PI) controller and a reference flux vector calculator (RFVC) do well to improve upon the torque response and the ripple effects [10].

In the execution of direct torque control, there is difficulty in keeping a constant switching frequency in operation. According to [2], a constant switching frequency is

achieved by comparison of a proportional-integral controller with a fixed frequency carrier signal. An outer loop PI regulator would govern the regulation of speed of the rotor and produce an output torque reference [19].

Direct Torque control has the following advantages over Field Oriented Control:

- There is no need for the measurement of rotor speed
- There is no need for transformation between different two-dimensional coordinate systems, since the d-q frame measurements are referred to the stator and are not rotating.
- As opposed to Field Oriented Control, Torque and flux are directly manipulated instead of control through the peripheral regulation of current in the direct and quadrature axes.
- There are significantly lower switching losses involved with direct torque control.
- There is no need for a position sensor to determine the angular rotor position in the motor, since there will be no implementation of the Inverse Park Transformation as described in equations (12) and (13).

There are different approaches to the implementation of direct torque control. The conventional approach involves the use of a switching table, where two adjacent voltage vectors are selected to manipulate the amplitude and phase angle of the resulting vector for stator flux [10]. Figure 9 and 10 below illustrate respectively, a switching table and the block diagram representation of direct torque control implementation via the use of the switching table with hysteresis comparators as controllers.

ϕ	τ	θ					
		$\theta(1)$	$\theta(2)$	$\theta(3)$	$\theta(4)$	$\theta(5)$	$\theta(6)$
$\phi = 1$	$\tau = 1$	$\mathbf{V}_2(110)$	$\mathbf{V}_3(010)$	$\mathbf{V}_4(011)$	$\mathbf{V}_5(001)$	$\mathbf{V}_6(101)$	$\mathbf{V}_1(100)$
	$\tau = 0$	$\mathbf{V}_6(101)$	$\mathbf{V}_1(100)$	$\mathbf{V}_2(110)$	$\mathbf{V}_3(010)$	$\mathbf{V}_4(011)$	$\mathbf{V}_5(001)$
$\phi = 0$	$\tau = 1$	$\mathbf{V}_3(010)$	$\mathbf{V}_4(011)$	$\mathbf{V}_5(001)$	$\mathbf{V}_6(101)$	$\mathbf{V}_1(100)$	$\mathbf{V}_2(110)$
	$\tau = 0$	$\mathbf{V}_5(001)$	$\mathbf{V}_6(101)$	$\mathbf{V}_1(100)$	$\mathbf{V}_2(110)$	$\mathbf{V}_3(010)$	$\mathbf{V}_4(011)$

Figure 9: Switching Table Used in Inverter Switching for Conventional DTC

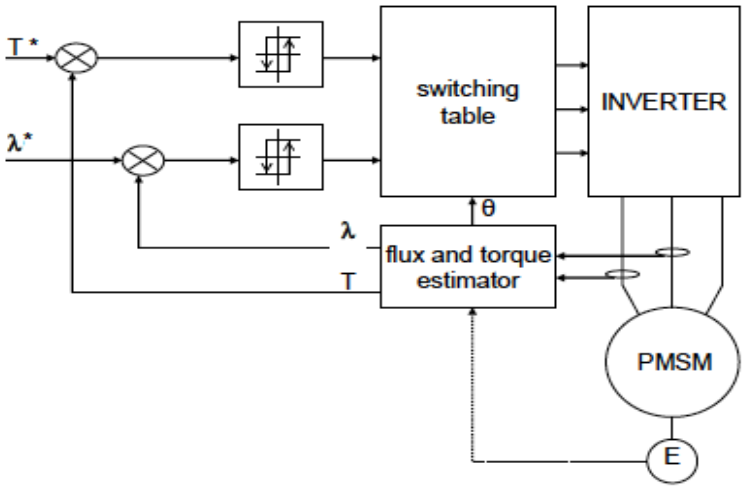

Figure 10: Block Diagram Representation of DTC with a Switching Table [10]

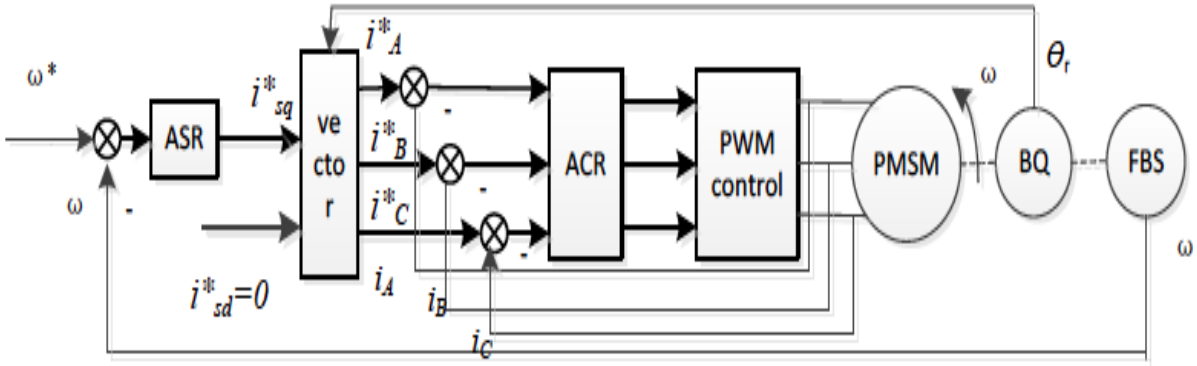

Figure 11: Modified Direct Torque Control with SVPWM & Current Control Loops [16]

Figure 11 illustrates the execution of direct torque control using Space Vector Modulation. With this process it can be seen that the feedback loops involve the stator winding currents and the angular speed of the rotor. This shows to be effective, since angular speed is shown to be directly proportional to flux, as shown in equations (1) and (2). The automatic speed regulator shown as a block receiving the error signal between measured and reference speed, and is characterized by a proportional-integral controller. The PI controller amplifies the error signal into a stator current reference, which is utilized in vector transformation and subsequent modulation.

Space Vector Pulse Width Modulation

The concept of space vector modulation was first engendered by inputs from Robert H. Park and Gabriel Kron in the early 1900s, but was mathematically developed a few decades later by K.P. Kovacs and J. Racz [14].

A space vector is a practical representation of a combination of separate phase vectors as a single vector. Space vector pulse width modulation is a form of pulse width modulation whereby a three-phase voltage vector is produced in the stator by a sequenced firing of the inverter switches connected to it. It has a similar dynamic of sequential gate firing of conventional pulse width modulation and is based on the selection of the two most adjacent vectors to be used in modulation.

Even though brushless DC (BLDC) motors do produce a trapezoidal back EMF, Figure 12 below exhibits the equivalent circuit of an inverter connected to a brushless dc motor. This circuit and connection represents a canon methodology that also applies to permanent magnet synchronous motors, as the only significant difference between both types of motor would be the back EMF produced. This owes to the higher winding concentration in BLDC motors [13].

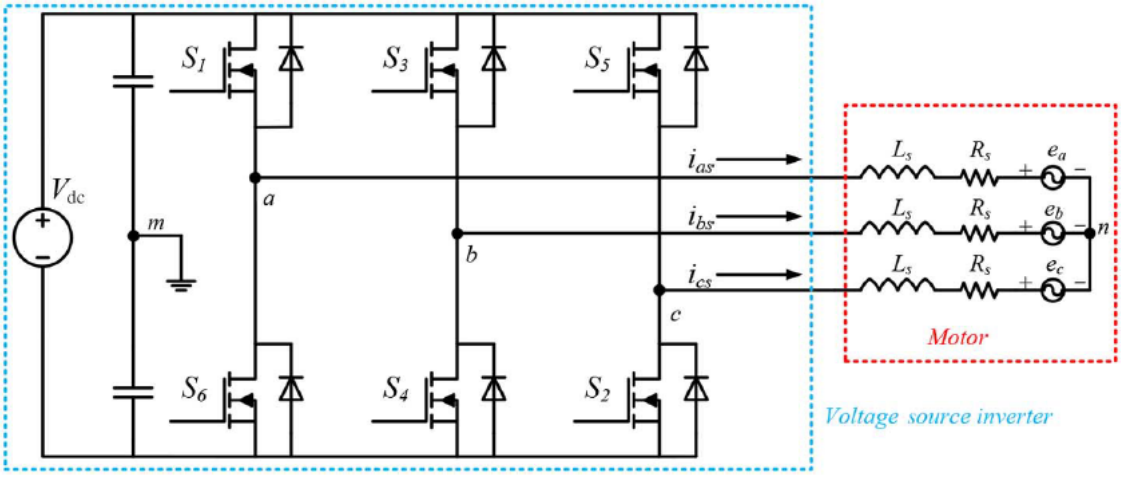

Figure 12: Three-Phase Inverter Coupled with a Generically Represented Brushless DC Motor with a Back-EMF [20]

With the constant rotation of stator magnetic flux, there exists a circular space-rotating field. This is mirrored as with vectors of voltage, whose rotating path is coincidental with that of the flux trajectory. The implementation of space vector pulse width modulation involves the use of six non-zero voltage vectors and two zero voltage vectors to generate a corresponding a circular flux to match that of the stator [11].

The mathematical representation of the space vector for stator voltage is expressed at an instant in time showing [15]:

$$\vec{v}_s^a(t) = v_a(t)e^{j0} + v_b(t)e^{-j2\pi/3} + v_c e^{j4\pi/3} \tag{22}$$

Referring to figure 12 and considering that:

$$e^{j0} + e^{j2\pi/3} + e^{j4\pi/3} = 0 \tag{23}$$

The space vector for the average stator voltage is then rewritten to be:

$$\vec{v}_s^a(t) = v_{aN}e^{j0} + v_{bN}e^{j2\pi/3} + v_{cN}e^{j4\pi/3} \tag{24}$$

Since the gate switches in figure 12 have a sequence of on and off states, we represent the on state of each switch by the number 1, and all off states by the number 0. This facilitates representation of the space vector below:

$$\vec{v}_s^a(t) = V_{dc}(q_a e^{j0} + q_b e^{j2\pi/3} + q_c e^{j4\pi/3}) \tag{25}$$

Seeing that there are two switch states for each of three phases, there exists a total of 2^3 possible combinations of on/off states between switches. Thus, the average stator voltage vector could be one of seven unique values at a given instant in time, where each value is a three digit binary number. Each digit is characterized by the state of the gate switch of each phase, a-b-c, from left to right. We therefore have resulting contributing voltage vectors to be [15]:

$$\begin{gathered}
\vec{v}_s^a(000) = \vec{v}_0 = 0 \\
\vec{v}_s^a(001) = \vec{v}_1 = V_d e^{j0} \\
\vec{v}_s^a(010) = \vec{v}_2 = V_d e^{j2\pi/3} \\
\vec{v}_s^a(011) = \vec{v}_3 = V_d e^{j\pi/3} \\
\vec{v}_s^a(100) = \vec{v}_4 = V_d e^{j4\pi/3} \\
\vec{v}_s^a(101) = \vec{v}_5 = V_d e^{j5\pi/3} \\
\vec{v}_s^a(110) = \vec{v}_6 = V_d e^{j\pi} \\
\vec{v}_s^a(111) = \vec{v}_7 = 0
\end{gathered} \tag{26}$$

Where $\vec{v}_0$ and $\vec{v}_7$ are zero vectors since their binary representations deem it so.

The vector voltages in equation (18) are hereafter referred to as "fundamental vectors". They form sectors of a plot shown in figure 10. It is noted that consecutive sectors only differ by a single digit or binary bit [15].

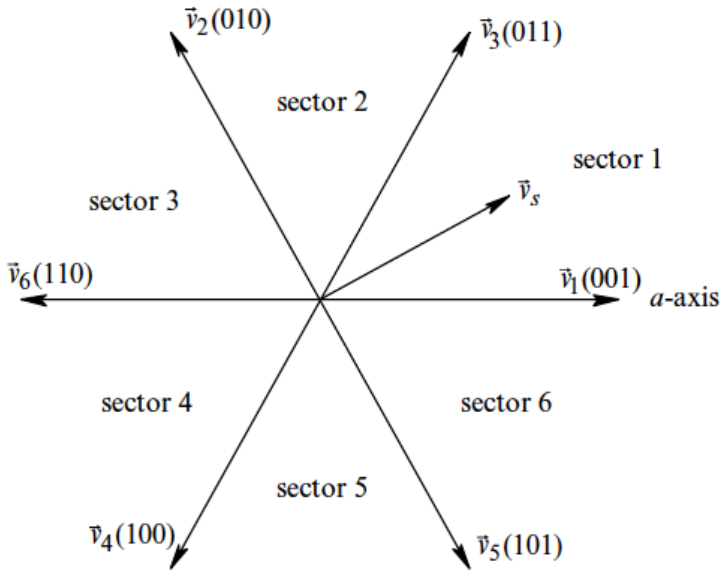

Figure 13: Plot of Sectors Created by Fundamental Voltage Space Vectors, sans Zero Vectors [15]

To achieve a successful space vector modulation, the aim boils down to the amalgamation of an average stator space voltage vector, $\vec{v}_s$, such that it acts as a reference. This contributes to a desired voltage output once the switching frequency remains constant, with minimal deviation from the reference, and the available voltage from the dc bus is as much as possible appropriated. In addition, it is desirable that the resulting ripple in current of the motor is mitigated as much as possible, with low switching losses from the inverter gates [15].

The fundamental voltage vectors are the key to the successful synthesis of the average stator voltage vector v_s, and the satisfaction of the conditions for a desirable voltage output. Two fundamental voltages within a sector are sampled along with the zero vectors, in order to effect a change in each transition of a state of one gate switch, in turn allowing minimum switching loss [15].

To illustrate the synthesis of the average voltage space vector $\vec{v}_s$, the operating principle is briefly analyzed with a focus on sector 1 in figure 10 as a generic example. Following this example in figure 11 below, $\vec{v}_s$ is averaged over a given period, 'T_s', using the adjacent fundamental vectors $\vec{v}_3$ and $\vec{v}_1$. The fundamentals are activated for intervals within the total period such that $\vec{v}_1$ is activated for xT_s seconds and $\vec{v}_3$ is activated for yT_s seconds. The zero vectors are also applied for zT_s seconds as well, and the resulting average voltage vector is then expressed as [15]:

$$\vec{v}_s^a = \frac{1}{T_s}[xT_s\vec{v}_1 + yT_s\vec{v}_3 + zT_s \cdot 0] \quad (27)$$

Where

$$x + y + z = 1 \quad (28)$$

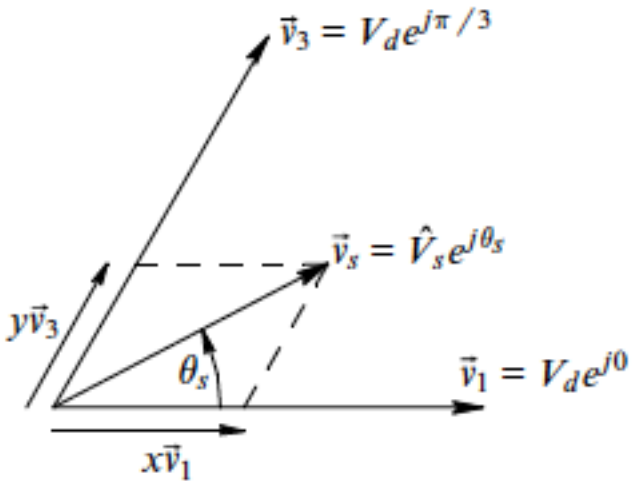

Figure 14: Synthesis of Average Voltage Vector in Sector 1

Substituting vector notation in (19) to illustrate voltage vectors in terms of amplitude and phase angle:

$$\vec{V}_s e^{j\theta_s} = xV_{dc}e^{j0} + yV_{dc}e^{j\pi/3} \quad (29)$$

The pattern of state switching is illustrated by figure 12 and details that phase a switches and remains on for the duration of the sum of xT_s, yT_s and zT_s periods. Phase c remains for the shortest period, and for every switch in states to a new sector, there is a change in state of only one phase/leg of the inverter. In figure 12, $z = z_0 + z_7$.

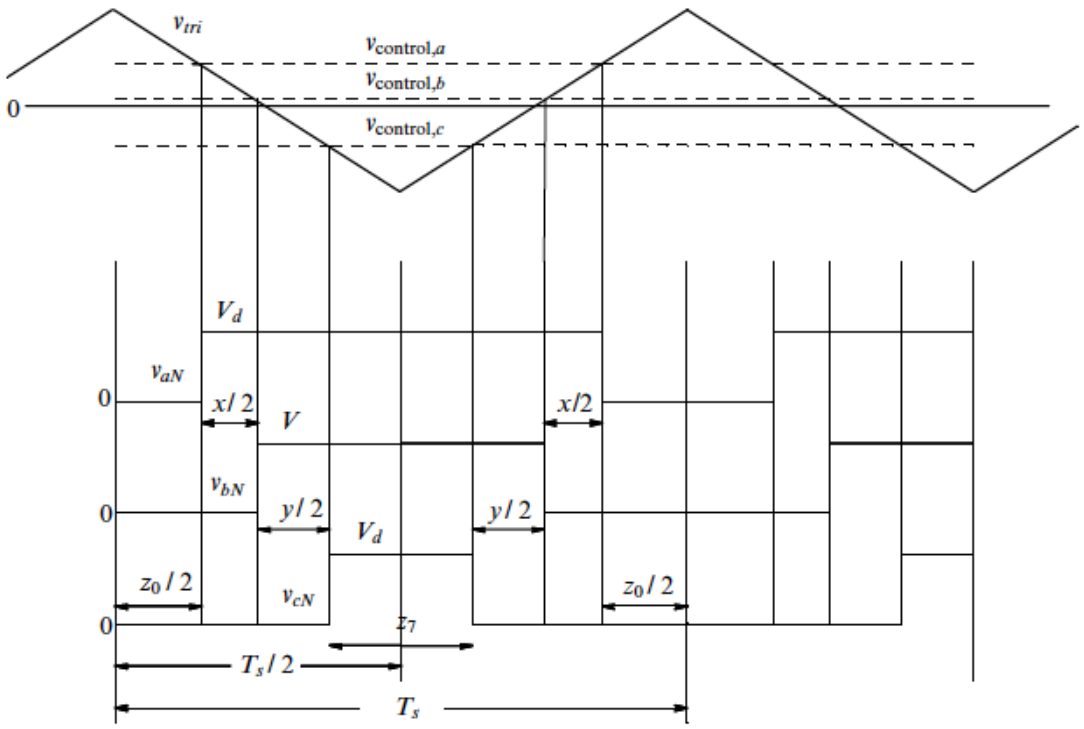

Figure 15: Waveforms of State Switching within Sector 1

An example of a simulation diagram for the generation of switching signals used in space vector modulation is shown in Figure 16 below [15]:

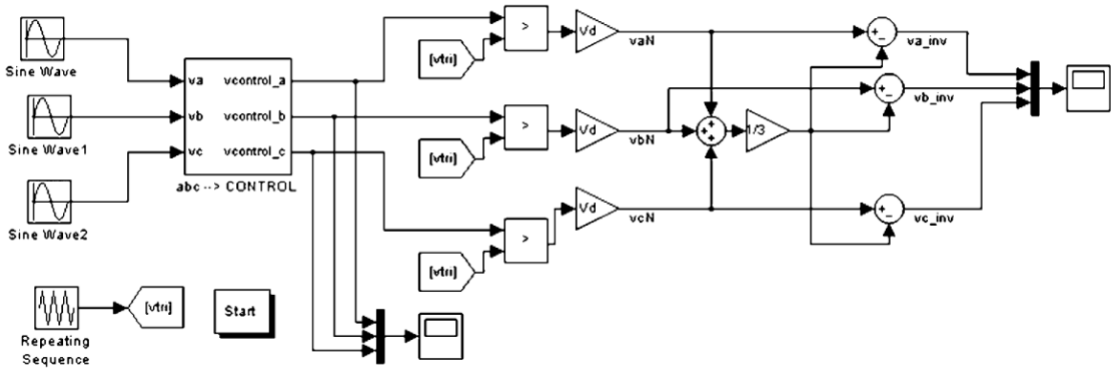

Figure 16: Simulation Block Diagram of Space Vector Modulation [15]

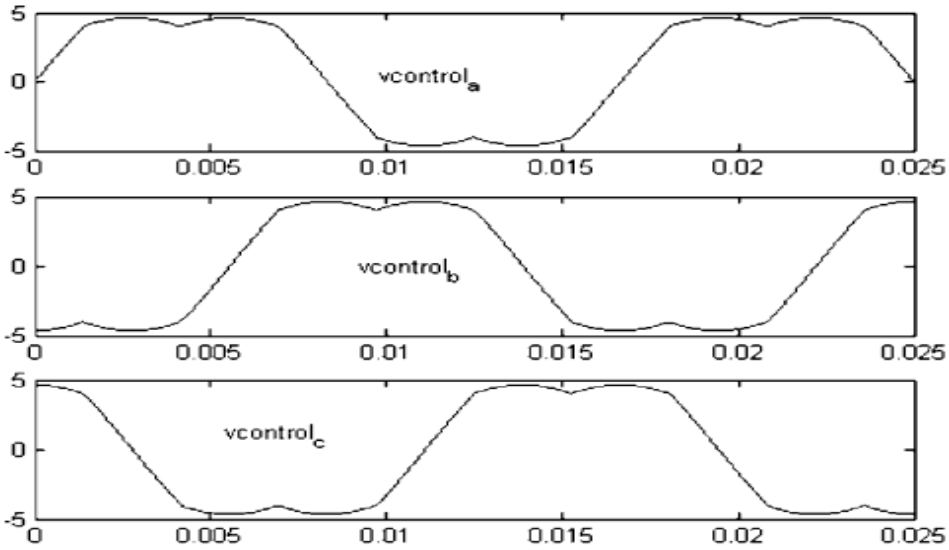

Figure 17: Output of Space Vector Modulation Simulation in Fig 16 [15]

CHAPTER 6

Simulation

Space Vector Pulse Width Modulation

First of all, a simulation is executed to implement the principles of space vector pulse width modulation, as studied in chapter 4. The full model shown in Figure 18 consists of an inverter controlled by space vector block. The system operated at a fundamental frequency of 60 Hz, with a switching frequency of 10 kHz and a modulation index of 0.8485. The Space Vector Modulation block takes effect upon receiving three sinusoidal voltage waveforms for each phase, which are then transformed into two-phase equivalent orthogonal components.

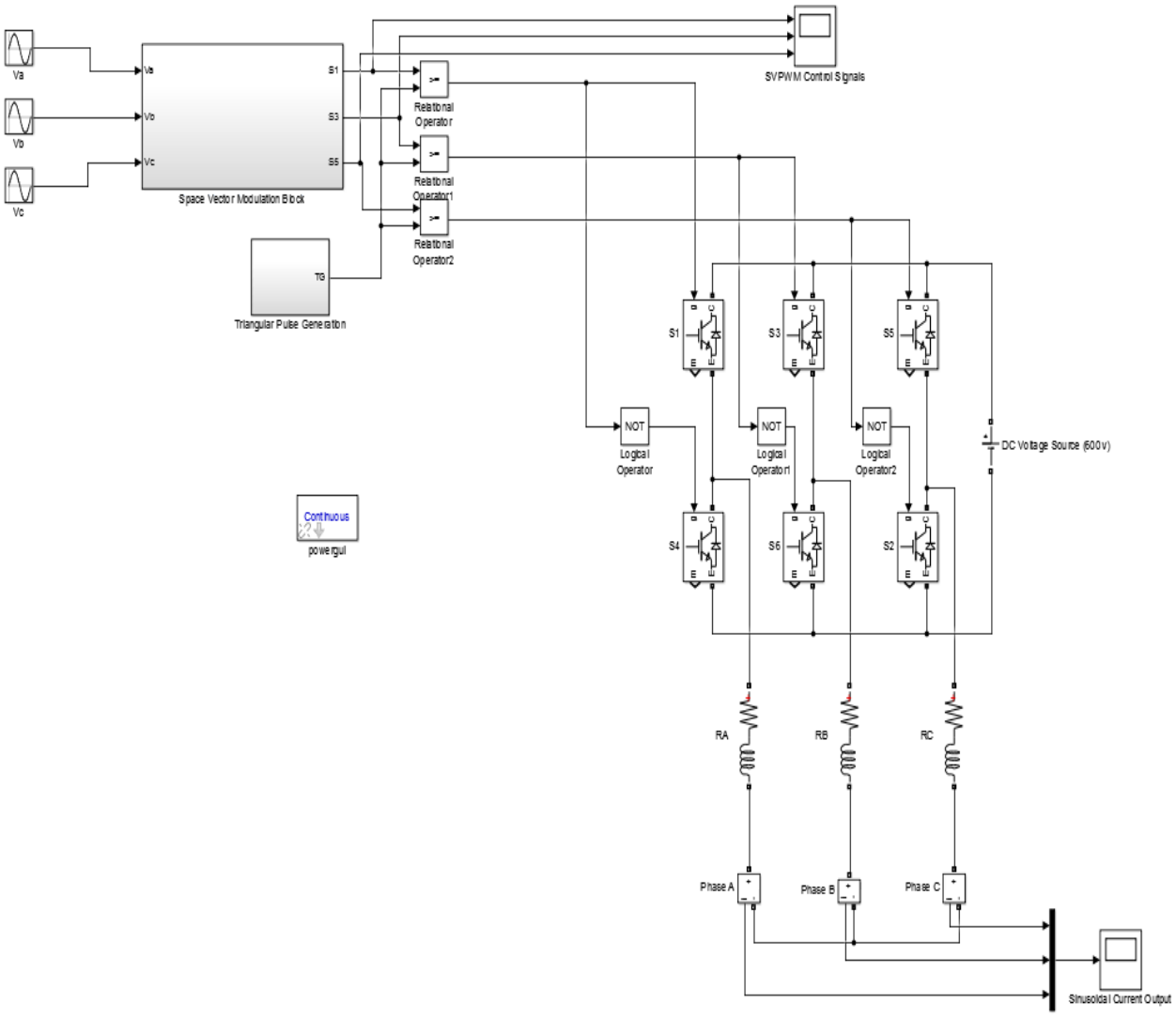

Figure 18: Full Simulation Diagram Executing SVPWM

In order to synthesize the average reference voltage vector, as well as regulate the duty cycle for modulation, the three-phase voltages are fed into a series of blocks that represent mathematical function models. These blocks were programmed in MATLAB accordingly. Codes for each block are shown in Figures 20 and 21.

The three voltage signals were transformed into the orthogonal two-axis rotating reference frame, as illustrated by the Clarke transformation matrix in equation (12). The two-axis voltage signals are used in calculating the average reference voltage vector using the instantaneous values obtained by the Clarke Transformation. The angle θ, created by the α and β voltages is also deduced and fed into the sector function block, which calculates the sector number within which the reference voltage is being averaged. The algorithm involved in this process is illustrated more clearly in Figure 20. Another angle used in the simulation was determined, as the difference between the angle θ and the reference voltage vector. The calculated reference voltage vector, together with the deduced angle ϕ and the switching period, serve as inputs to a function that estimated the switching times required for the transistor gate switching duty cycle. The switching periods calculated are then compared with the switching period of the triangular ramp and these determine the sequence of switching within the inverter.

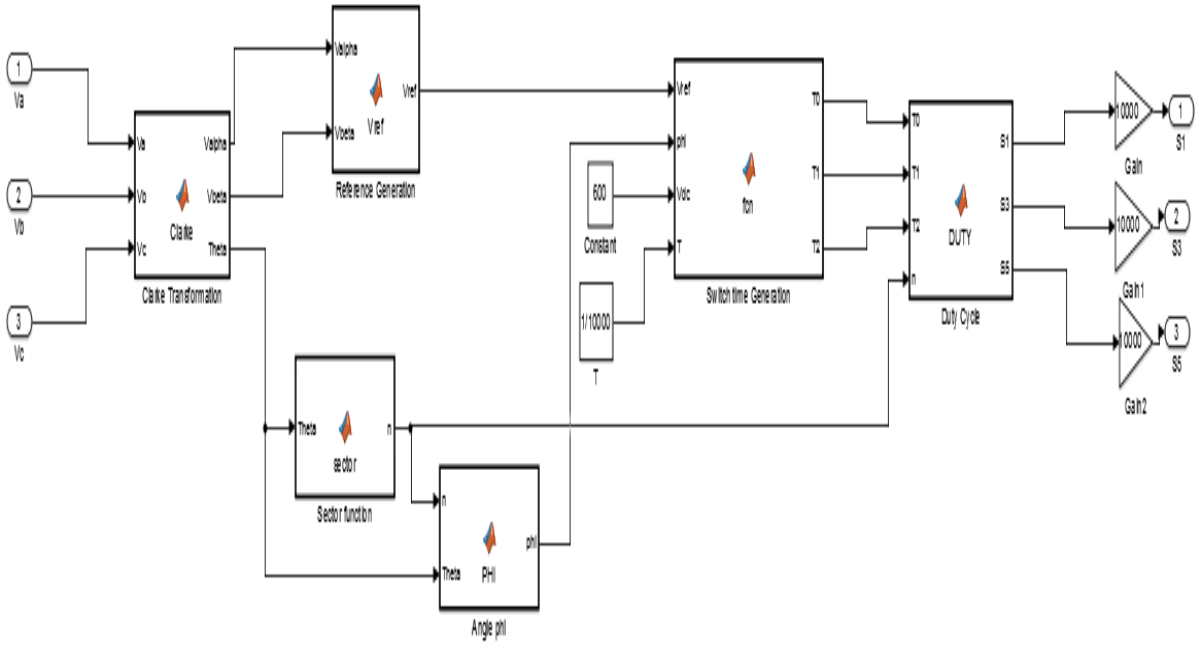

Figure 19: Inner Configuration of Space Vector Modulation Block

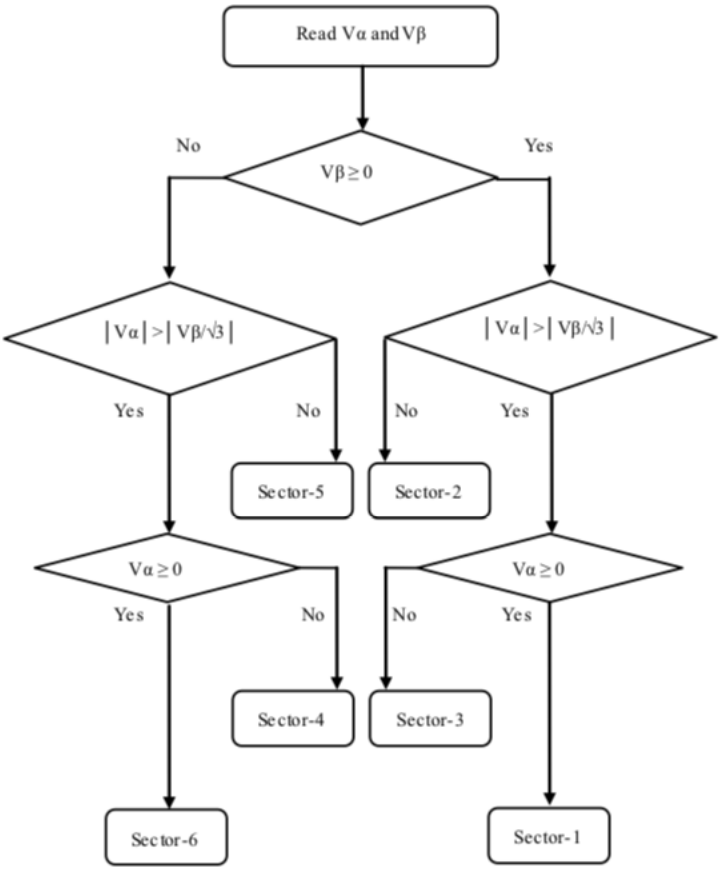

Figure 20: Flow Chart of Sector Number Determination based on V_α & V_β [18]

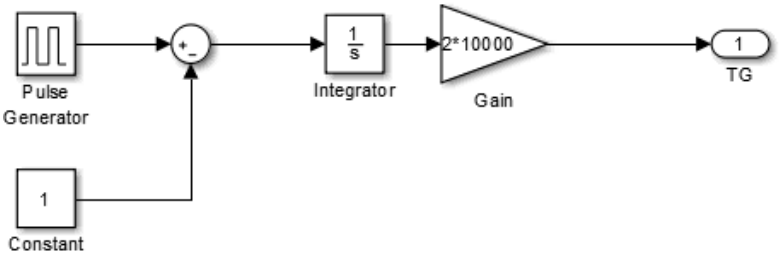

Figure 21: Inner Configuration of Triangular Pulse Generation Bloc

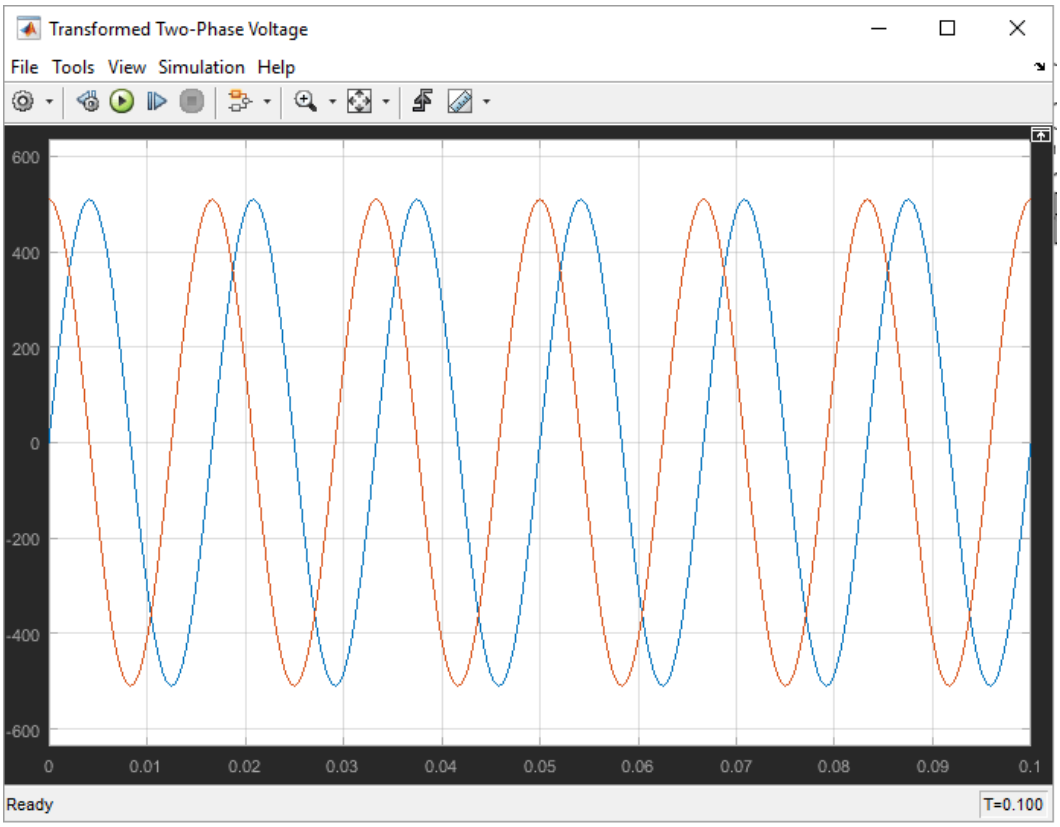

Figure 22: Output of Voltages Transformed from 3-phase to Two-Phase

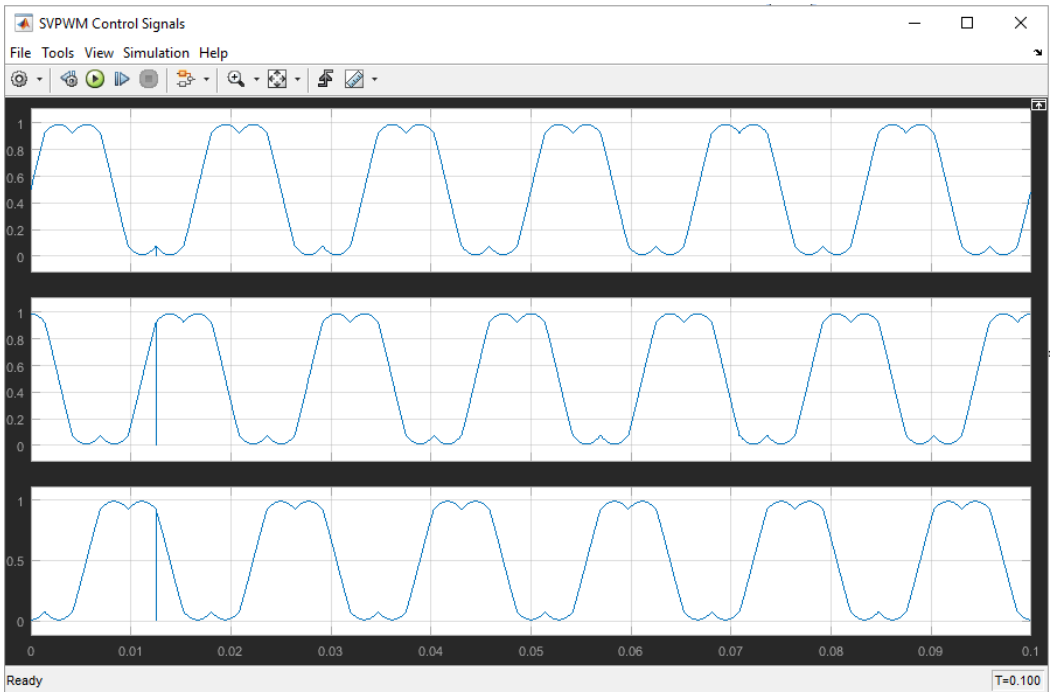

Figure 23: Output of Switching Signals into the Inverter (S1, S3, S5)

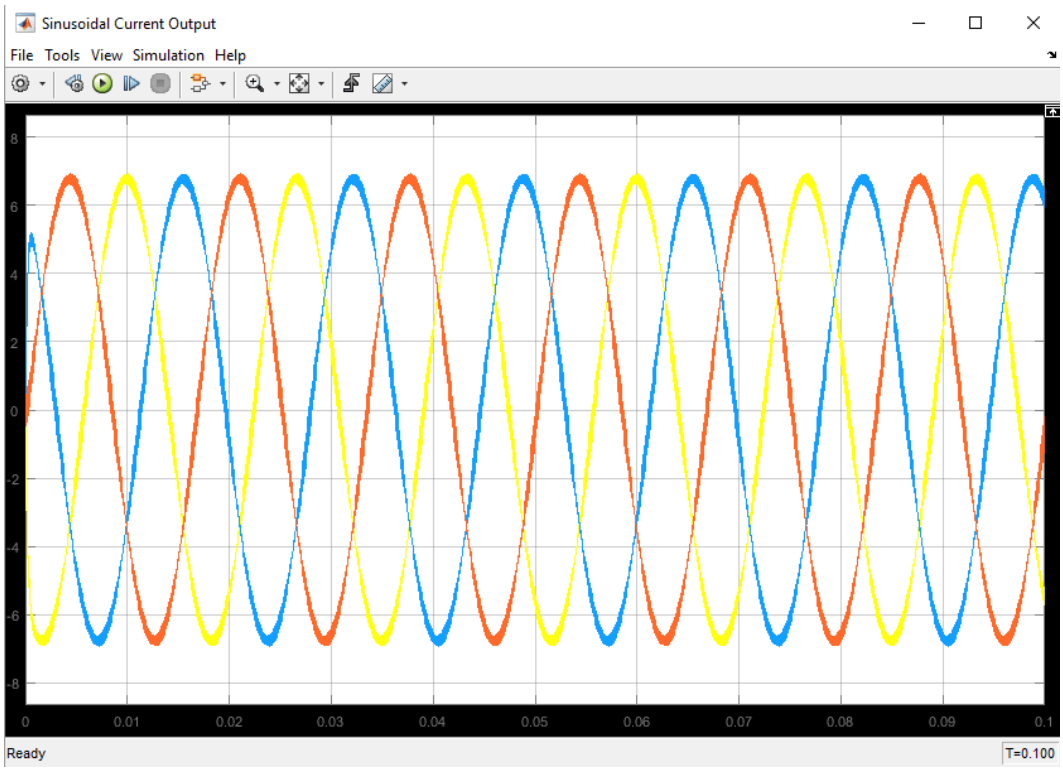

Figure 24: Output of Sinusoidal Three-Phase Current to the Load

Space Vector Modulation Block/Clarke Transformation

```
function [Valpha,Vbeta,Theta] = Clarke(Va,Vb,Vc)
Valpha=Va-Vb/2-Vc/2;
Vbeta=sqrt(3)/2*(Vb-Vc);
Theta=atan2(Vbeta,Valpha);
```

Space Vector Modulation Block/Reference Generation

```
function Vref = Vref(Valpha,Vbeta)
Vref=sqrt(Valpha^2+Vbeta^2);
```

Space Vector Modulation Block/Switch time Generation

```
function [T0,T1,T2] = fcn(Vref,phi,Vdc,T)
a=Vref/Vdc
T1=T*a*sin(pi/3-phi)/sin(pi/3);
T2=T*a*sin(phi)/sin(pi/3);
T0=T-T1-T2;
```

Space Vector Modulation Block/Sector function

```
function n = sector(Theta)
n=0;
if(Theta>0)&(Theta<=pi/3)
    n=1;
end;
if (Theta>pi/3)&(Theta<=2*pi/3)
    n=2;
end;
if(Theta>2*pi/3)&(Theta<=pi)
    n=3;
end;
if(Theta<=0)&(Theta>-pi/3)
    n=6;
end;
if(Theta<=-pi/3)&(Theta>-2*pi/3)
    n=5;
end;
if(Theta<=-2*pi/3)&(Theta>-pi)
    n=4;
end;
```

Figure 25: MATLAB Codes for Clarke Transformation, Voltage Reference Generation, Switching Time Calculation, and Sector Number Function Blocks

Space Vector Modulation Block/Angle phi

```
function phi = PHI(n,Theta)
phi=0;
if(n==1)
    phi=Theta;
end;
if(n==2)
    phi=Theta-pi/3;
end;
if(n==3);
    phi=Theta-2*pi/3;
end;
if(n==6)
    phi=pi/3+Theta;
end;
if(n==5)
    phi=2*pi/3+Theta;
end;
if(n==4)
    phi=pi+Theta;
end;
```

```
function [S1,S3,S5] = DUTY(T0,T1,T2,n)
S1=0;
S3=0;
S5=0;
if(n==1)
    S1=T1+T2+T0/2;
    S3=T2+T0/2;
    S5=T0/2;
end;
if(n==2)
    S1=T1+T0/2;
    S3=T1+T2+T0/2;
    S5=T0/2;
end;
if(n==3)
    S1=T0/2;
    S3=T1+T2+T0/2;
    S5=T2+T0/2;
end;
if(n==4)
    S1=T0/2;
    S3=T1+T0/2;
    S5=T1+T2+T0/2;
end;
if(n==5)
    S1=T2+T0/2;
    S3=T0/2;
    S5=T1+T2+T0/2;
end;
if(n==6)
    S1=T1+T2+T0/2;
    S3=T0/2;
    S5=T1+T0/2;
end;
```

Figure 26: MATLAB Codes for ϕ Angle and Duty Cycle Calculations

Permanent Magnet Synchronous Motor With Direct Torque Control

The motor drive model under consideration encompassed the simulation of the operation of the permanent magnet synchronous motor perturbed by changes in load torque with time. It began with a 400 dc-link-voltage IGBT-based inverter that was fed into a three-phase salient pole permanent magnet synchronous motor with a sinusoidal back-EMF. The measuring signal terminal output the machine's stator current in the d and q frame, electromagnetic torque produced, and the speed of the rotor with changing conditions. The rotor angle of the shaft was also measured, but only as it was required for one of the two feedback loops involved.

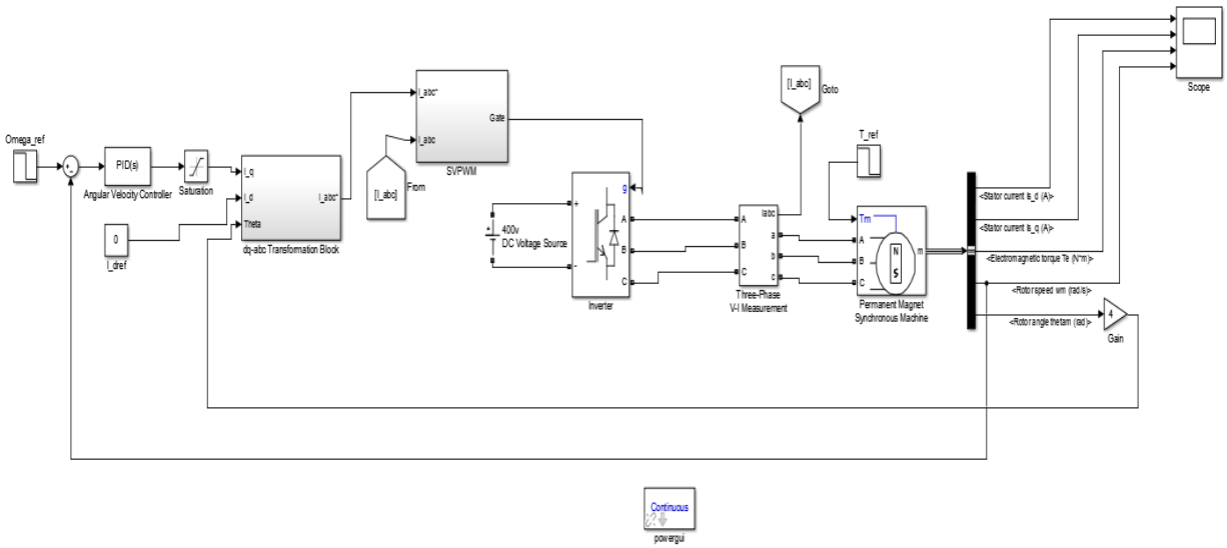

Figure 27: Simulink Block Diagram of PMSM Direct Torque Control

The first feedback was important for the compensation in deviation of rotor speed, which was required to gauge the response of the machine speed to changes in load torque. Here the measured speed of the rotor was compared with a reference speed, and the sum that was produced in the comparison was then fed into a PID controller for increased efficacy. The resulting signal was then amplified to produce a reference stator current for transformation into three-phase, and further modulation for the inverter gate signals.

A position sensor was imitated by measuring the rotor angle, θ, which was then an input to the d-q to a-b-c transformation into vectors for space vector pulse-width modulation.

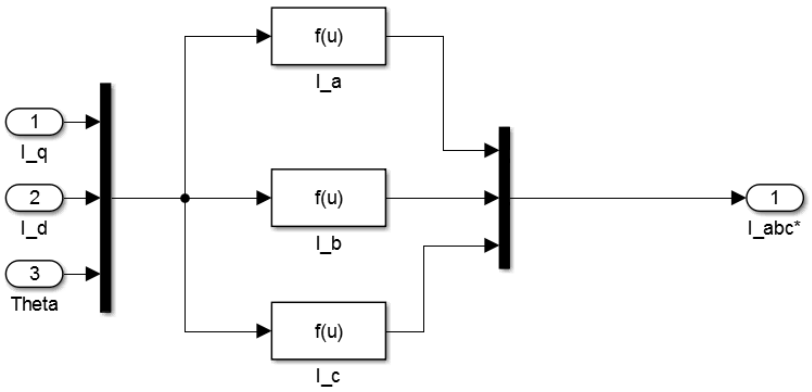

Figure 28: Internal Components of Transformation Block

Seeing as the control of three-phase stator vector current depends heavily on the location of the rotor shaft by virtue of it's angle, the transformation block simply consists of a set of functions that emulate the transformation equations shown below:

$$i_a = i_q \cos\theta - i_d \sin\theta \tag{14}$$

$$i_b = i_q \cos(\theta - {}^{2}/_{3}\,\pi) - i_d \sin(\theta - {}^{2}/_{3}\,\pi) \tag{15}$$

$$i_c = i_q \cos(\theta + {}^{2}/_{3}\,\pi) - i_d \sin(\theta + {}^{2}/_{3}\,\pi) \tag{16}$$

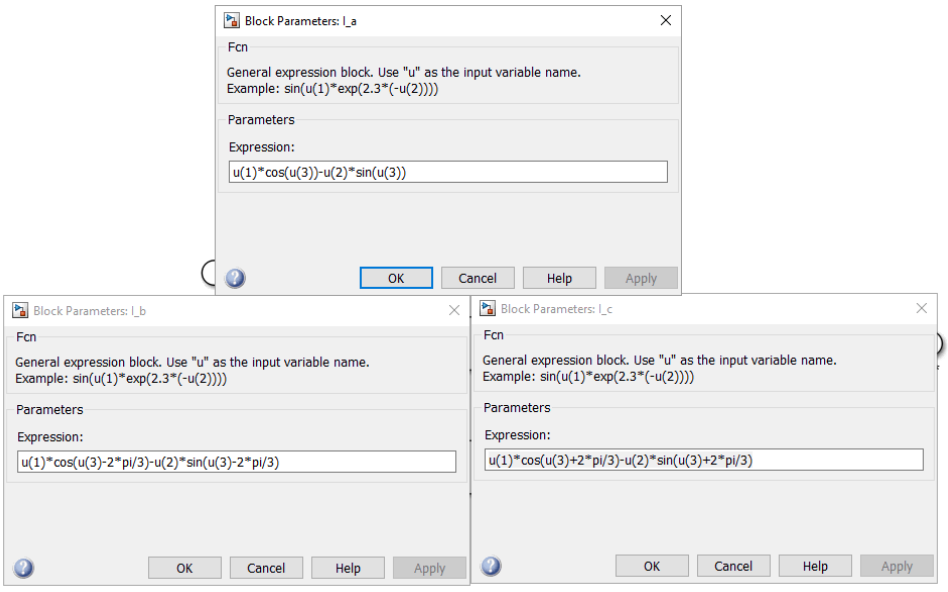

Figure 29: Function Block Parameters for dq-abc Transformation

Since the direct axis is closely related to flux and the quadrature to torque, there is no need for a d-axis reference here, as the torque is the parameter of interest here. The transformed vector was then fed into the space vector pulse width modulation block model, which consisted of a set of relays that fired sequentially in comparison with the initially measured three-phase currents of the machine. The modulated signal was fed back into the gates of the inverter, which completed the feedback.

The simulation was ran for 1 second, and was initially running under regular loaded conditions until 0.3 seconds, when mechanical torque input was reduced to simulate an increase in load. The outputs of the above simulation are shown below, displaying the behavior of q-axis stator current, angular rotor speed and electromagnetic torque. As can be observed in figure 14 below, the machine under initial load conditions, reaches steady state after an initial perturbation in about 0.22 seconds, and then is further disturbed when the load is increased. The current experiences a ripple as it goes into steady state and then dips as the load changes. Another ripple is experienced before a final steady state is approached.

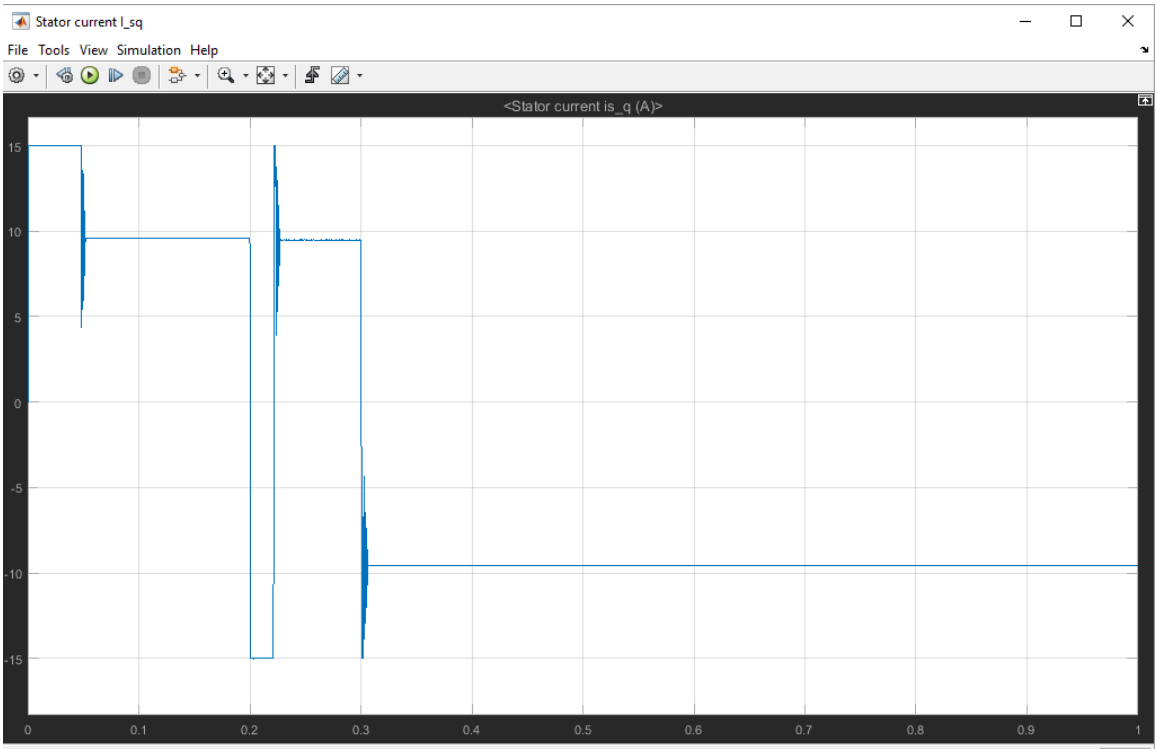

Figure 30: Output of q-axis Stator Current

In figure 15, the response of the rotor speed was observed, although it experienced a slight movement about the change in load, the overall change in load did not cause much of a change in speed after it reached steady state. This may be as a result of the fact that speed changes with change in load and therefore the increase in load

caused a commensurate change in load speed and therefore did not exhibit a large net deviation.

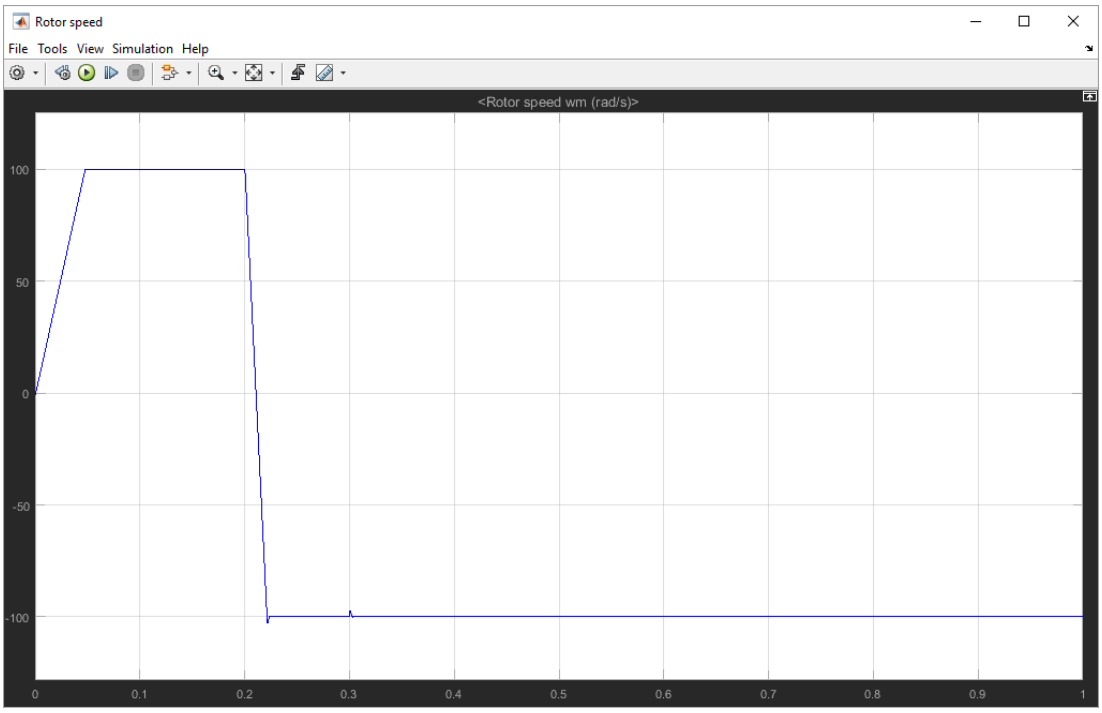

Figure 31: Output of Rotor Speed with Change in Load

Figure 16 below exhibits the changes in torque at the output of the machine, where it can be observed that the torque experienced a disturbance but achieved a steady output right before the load was changed. The net load torque then fell, where a ripple can be observed at the point where a steady state was achieved.

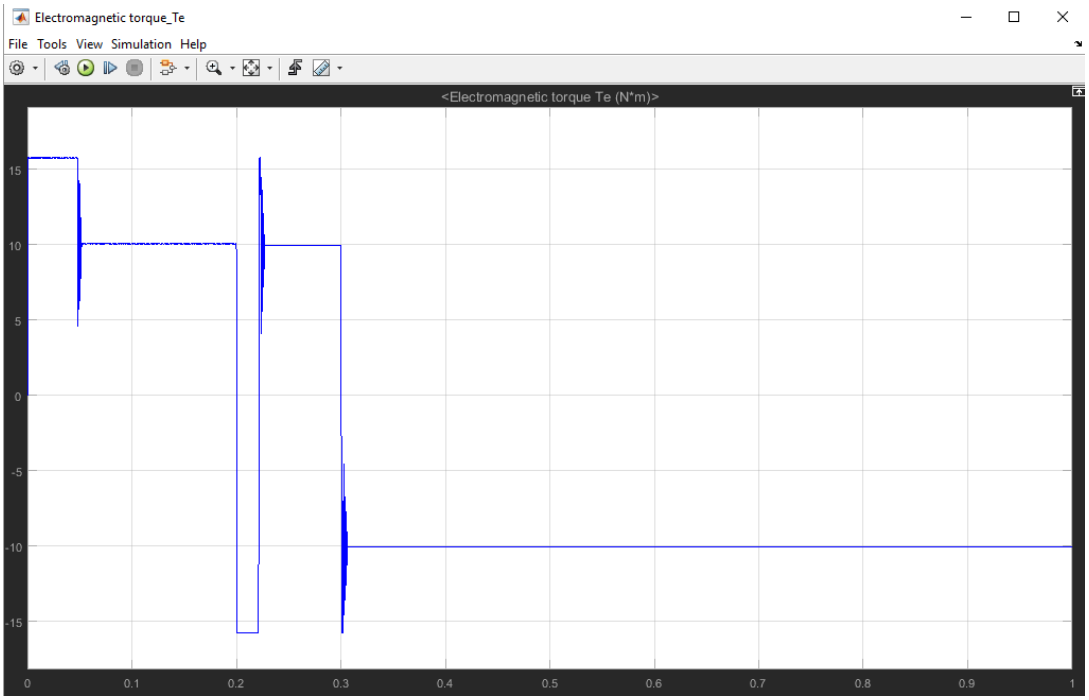

Figure 32: Output of Electromagnetic Torque Produced

Evidently, the final steady state achieved is not at its most stable, as some residual harmonic ripples can be seen after 0.3 seconds.

CONCLUSION

In this paper, the characteristics of direct torque control and field-oriented control were analyzed and weighed against each other. Due to the complex nature and volatile sensitivity of field-oriented control to parameter and load torque variations, only direct torque was simulated using MATLAB/Simulink. Replacing the conventional look-up table with space vector modulation, however, modified the iterative algorithm applied to the simulation. This is because the switching table would exacerbate torque ripples in the event of varying parameters of the motor drive or variation in load.

The changes in load in the simulation demonstrated the system response as previously shown in the figures, with slight transient ripples in torque. Deviations were offset by the implementation of a PI controller, which provided a reference torque for steady state. The controller was also responsible for maintaining a constant speed after stability was established. The variation in load therefore demonstrated a semblance of resilience as opposed to conventional direct torque by the use of switching tables.

Space vector modulation was also explored and demonstrated, exhibiting the maintenance of a nearly constant switching frequency, which takes part responsibility for the robust response to changing load conditions. A simple simulation of space vector modulation successfully exhibited its operation.

REFERENCES

[1] J. Liu, H. Li and Y. Deng, "Torque Ripple Minimization of PMSM Based on Robust ILC Via Adaptive Sliding Mode Control," in *IEEE Transactions on Power Electronics*, vol. 33, no. 4, pp. 3655-3671, April 2018.

[2] X. Zhang and G. H. B. Foo, "A Constant Switching Frequency-Based Direct Torque Control Method for Interior Permanent-Magnet Synchronous Motor Drives," in *IEEE/ASME Transactions on Mechatronics*, vol. 21, no. 3, pp. 1445-1456, June 2016.

[3] Weizhe Qian, S. K. Panda and Jian-Xin Xu, "Torque ripple minimization in PM synchronous motors using iterative learning control," in *IEEE Transactions on Power Electronics*, vol. 19, no. 2, pp. 272-279, March 2004.

[4] J. Holtz and L. Springob, "Identification and compensation of torque ripple in high-precision permanent magnet motor drives," in *IEEE Transactions on Industrial Electronics*, vol. 43, no. 2, pp. 309-320, Apr 1996.

[5] "Field Orientated Control of 3-Phase AC-Motors," Texas Instruments Europe, 1998, pp. 1-14.

[6] A. M. Bozorgi, M. Farasat and S. Jafarishiadeh, "Model predictive current control of surface-mounted permanent magnet synchronous motor with low torque and current ripple," in *IET Power Electronics*, vol. 10, no. 10, pp. 1120-1128, 8 18 2017.

[7] T. M. Jahns and W. L. Soong, "Pulsating torque minimization techniques for permanent magnet AC motor drives-a review," in *IEEE Transactions on Industrial Electronics*, vol. 43, no. 2, pp. 321-330, Apr 1996.

[8] V. M. Bida, D. V. Samokhvalov and F. S. Al-Mahturi, "PMSM vector control techniques — A survey," *2018 IEEE Conference of Russian Young Researchers in Electrical and Electronic Engineering (EIConRus)*, Moscow and St. Petersburg, Russia, 2018, pp. 577-581.

[9] M. F. Rahman, L. Zhong, W. Y. Hu, K. W. Lim and M. A. Rahman, "A direct torque controller for permanent magnet synchronous motor drives," *1997 IEEE International Electric Machines and Drives Conference Record*, Milwaukee, WI, 1997, pp. TD1/2.1-TD1/2.3.

[10] M. A. Said, M. F. M. Elias, H. W. Ping and N. A. Rahim, "Switching-table and space vector modulation direct torque control of permanent magnet synchronous motor drives simulation," *2009 International Conference for Technical Postgraduates (TECHPOS)*, Kuala Lumpur, 2009, pp. 1-4.

[11] J. P. John, S. S. Kumar and B. Jaya, "Space Vector Modulation based Field Oriented Control scheme for Brushless DC motors," *2011 International Conference on Emerging Trends in Electrical and Computer Technology*, Tamil Nadu, 2011, pp. 346-351.

[12] J. Lara, J. Xu and A. Chandra, "Effects of Rotor Position Error in the Performance of Field-Oriented-Controlled PMSM Drives for Electric Vehicle Traction Applications," in *IEEE Transactions on Industrial Electronics*, vol. 63, no. 8, pp. 4738-4751, Aug. 2016.

[13] P. Pillay and R. Krishnan, "Application characteristics of permanent magnet synchronous and brushless DC motors for servo drives," in *IEEE Transactions on Industry Applications*, vol. 27, no. 5, pp. 986-996, Sep/Oct 1991.

[14] Neacsu, D.O. "Space vector modulation - An introduction" - Tutorial at IECON, 2001.

[15] Ned Mohan, “Advanced Electric Drives: Analysis, Control, and Modeling Using MATLAB/Simulink®, First Edition. “ 2014 John Wiley & Sons, Inc. Published 2014 by John Wiley & Sons, Inc.

[16] Y. Liu, Z. Zhang “PMSM Control System Research Based on Vector Control” in *International Conference on Information Sciences, Machinery, Materials and Energy (ICISMME)*, 2015.

[17] Sun Dan “Clarke’s and Park’s Transformations” College of Engineering, Zhejiang University, BPRA047,BPRA048, 2008.

[18] Waheed Ahmed and Syed M Usman Ali “Comparative study of SVPWM (space vector pulse width modulation) & SPWM (sinusoidal pulse width modulation) based three phase voltage source inverters for variable speed drive” 2013 *IOP Conf. Ser.: Mater. Sci. Eng.* **51** 012027.

[19] Y. Fan, L. Zhang, M. Cheng and K. T. Chau, "Sensorless SVPWM-FADTC of a New Flux-Modulated Permanent-Magnet Wheel Motor Based on a Wide-Speed Sliding Mode Observer," in *IEEE Transactions on Industrial Electronics*, vol. 62, no. 5, pp. 3143-3151, May 2015.

[20] F. Yang, A. R. Taylor, H. Bai, B. Cheng and A. A. Khan, "Using d–q Transformation to Vary the Switching Frequency for Interior Permanent Magnet Synchronous Motor Drive Systems," in *IEEE Transactions on Transportation Electrification*, vol. 1, no. 3, pp. 277-286, Oct. 2015.